

# Histogram of Gradient Orientations of Signal Plots applied to P300 Detection

Rodrigo Ramele<sup>1\*</sup>, Ana J. Villar<sup>1</sup>, Juan M. Santos<sup>1</sup>

<sup>1</sup>Computer Engineering Department, Instituto Tecnológico de Buenos Aires, Argentina

*Submitted to Journal:*  
Frontiers in Computational Neuroscience

*Article type:*  
Original Research Article

*Manuscript ID:*  
357255

*Received on:*  
30 Jan 2018

*Frontiers website link:*  
[www.frontiersin.org](http://www.frontiersin.org)

### *Conflict of interest statement*

The authors declare that the research was conducted in the absence of any commercial or financial relationships that could be construed as a potential conflict of interest

### *Author contribution statement*

This work is part of the PhD thesis of RR which is directed by JS and codirected by AV.

### *Keywords*

Electroencephalography, histogram of gradient orientations, Brain-Computer Interfaces, P300, SIFT, Amyotrophic Lateral Sclerosis, naive-bayes near neighbours, waveform

### *Abstract*

Word count: 179

The analysis of Electroencephalographic (EEG) signals is of ulterior importance for decoding patterns that could improve the implementation of Brain Computer Interfaces (BCI). These systems are meant to provide alternative pathways to transmit volitional information which could potentially enhance the quality of life of patients affected by neurodegenerative disorders and other mental illness. Of particular interests are those which are based on the recognition of Event-Related Potentials (ERP) because they can be elicited by external stimuli and used to implement spellers, to control external devices or even avatars in virtual reality environments. This work mimics what electroencephalographers have been doing clinically, visually inspecting and categorizing phenomena within the EEG by the extraction of features from the images of the plots of the signals. It also aims to provide a framework to analyze, characterize and classify EEG signals, with a focus on the P300, an ERP elicited by the oddball paradigm of rare events. The validity of the method is shown by offline processing a public dataset of Amyotrophic Lateral Sclerosis (ALS) patients and an own dataset of healthy subjects.

### *Funding statement*

This project was supported by the ITBACyT-15 funding program issued by ITBA University from Buenos Aires, Argentina.

### *Ethics statements*

(Authors are required to state the ethical considerations of their study in the manuscript, including for cases where the study was exempt from ethical approval procedures)

*Does the study presented in the manuscript involve human or animal subjects:* Yes

*Please provide the complete ethics statement for your manuscript. Note that the statement will be directly added to the manuscript file for peer-review, and should include the following information:*

- Full name of the ethics committee that approved the study
- Consent procedure used for human participants or for animal owners
- Any additional considerations of the study in cases where vulnerable populations were involved, for example minors, persons with disabilities or endangered animal species

*As per the Frontiers authors guidelines, you are required to use the following format for statements involving human subjects: This study was carried out in accordance with the recommendations of [name of guidelines], [name of committee]. The protocol was approved by the [name of committee]. All subjects gave written informed consent in accordance with the Declaration of Helsinki.*

*For statements involving animal subjects, please use:*

*This study was carried out in accordance with the recommendations of 'name of guidelines, name of committee'. The protocol was approved by the 'name of committee'.*

*If the study was exempt from one or more of the above requirements, please provide a statement with the reason for the*

*exemption(s).*

*Ensure that your statement is phrased in a complete way, with clear and concise sentences.*

Participants are recruited voluntarily and the experiment is conducted anonymously in accordance with the declaration of Helsinki published by the World Health Organization. No monetary compensation is handed out and all participants agree and sign a written informed consent approved by the ITBA University Research Commission.

In review

# Histogram of Gradient Orientations of Signal Plots applied to P300 Detection

Rodrigo Ramele<sup>1,\*</sup>, Ana Julia Villar<sup>1</sup> and Juan Miguel Santos<sup>1</sup>

<sup>1</sup>*Centro de Inteligencia Computacional, Computer Engineering Department,  
Instituto Tecnológico de Buenos Aires, Buenos Aires, Argentina*

Correspondence\*:

Rodrigo Ramele, C1437FBH Lavarden 315, Ciudad Autónoma de Buenos Aires,  
Argentina  
rramele@itba.edu.ar

## 2 ABSTRACT

3 Word Count: 4841

4 The analysis of Electroencephalographic (EEG) signals is of ulterior importance for decoding  
5 patterns that could improve the implementation of Brain Computer Interfaces (BCI). These  
6 systems are meant to provide alternative pathways to transmit volitional information which could  
7 potentially enhance the quality of life of patients affected by neurodegenerative disorders and  
8 other mental illness. Of particular interests are those which are based on the recognition of  
9 Event-Related Potentials (ERP) because they can be elicited by external stimuli and used to  
10 implement spellers, to control external devices or even avatars in virtual reality environments.  
11 This work mimics what electroencephalographers have been doing clinically, visually inspecting  
12 and categorizing phenomena within the EEG by the extraction of features from images of signal  
13 plots. It also aims to provide a framework to analyze, characterize and classify EEG signals, with  
14 a focus on the P300, an ERP elicited by the oddball paradigm of rare events. The validity of the  
15 method is shown by offline processing a public dataset of Amyotrophic Lateral Sclerosis (ALS)  
16 patients and an own dataset of healthy subjects.

17 **Keywords:** electroencephalography, histogram of gradient orientations, brain-computer interfaces, P300, SIFT, amyotrophic lateral  
18 sclerosis, naive-bayes near neighbours, waveforms

## 1 INTRODUCTION

19 Although recent advances in neuroimaging techniques, particularly radio-nuclear and radiological  
20 scanning methods (Schomer and Silva, 2010), have diminished the prospects of the traditional  
21 Electroencephalography (EEG), the advent and development of digitized devices has impelled for a  
22 revamping of this hundred years old technology. Their versatility, ease of use, temporal resolution, ease of  
23 development and production, and its proliferation as consumer devices, are pushing EEG to become the  
24 de-facto non invasive portable or ambulatory method to access and harness brain information (De Vos and  
25 Debener, 2014).

26 A key contribution to this expansion has been the field of Brain Computer Interfaces (BCI) (Wolpaw and  
27 E., 2012) which is the pursuit of the development of a new channel of communication particularly aimed to  
28 persons affected by neurodegenerative diseases.

One noteworthy aspect of this novel communication channel is the ability to transmit information from the Central Nervous System (CNS) to a computer device and from there use that information to control a wheelchair (Carlson and del R. Millan, 2013), as input to a speller application (Guger et al., 2009), in a Virtual Reality environment (Lotte et al., 2013) or as aiding tool in a rehabilitation procedure (Jure et al., 2016). The holly grail of BCI is to implement a new complete and alternative pathway to restore lost locomotion (Wolpaw and E., 2012).

EEG signals are remarkably complex and have been characterized as a multichannel non-stationary stochastic process. Additionally, they have high variability between different subjects and even between different moments for the same subject, requiring adaptive and co-adaptive calibration and learning procedures (Clerc et al., 2016). Hence, this imposes an outstanding challenge that is necessary to overcome in order to extract information from raw EEG signals.

BCI has gained mainstream public awareness with worldwide challenge competitions like Cybathlon (Riener and Seward, 2014; Novak et al., 2018) and even been broadcasted during the inauguration ceremony of the 2014 Soccer World Cup. New developments have overcome the out-of-the-lab high-bar and they are starting to be used in real world environments (Guger et al., 2017; Huggins et al., 2016). However, they still lack the necessary robustness, and its performance is well behind any other method of human computer interaction, including any kind of detection of residual muscular movement (Clerc et al., 2016).

A few works have explored the idea of exploiting the signal waveform to analyze the EEG signal. In (Alvarado-González et al., 2016) an approach based on Slope Horizontal Chain Code is presented, whereas in (Yamaguchi et al., 2009) a similar procedure was implemented based on Mathematical Morphological Analysis. The seminal work of Bandt-Pompe Permutation Entropy (Berger et al., 2017) also explores succinctly this idea as a basis to establish the time series ordinal patterns. In the article (Ramele et al., 2016), the authors introduce a method for classification of rhythmic EEG events like Visual Occipital Alpha Waves and Motor Imagery Rolandic Central  $\mu$  Rhythms using the histogram of gradient orientations of signal plots. Inspired in that work, we propose a novel application of the developed method to classify and describe transient events, particularly the P300 Event Related Potential. The proposed approach is based on the waveform analysis of the shape of the EEG signal, but using histogram of gradient orientations. The method is built by mimicking what traditionally electroencephalographers have been performing for almost a century as it is described in (Hartman, 2005): visually inspecting raw signal plots.

This paper reports a method to, (1) describe a procedure to capture the shape of a waveform of an ERP component, the P300, using histograms of gradient orientations extracted from images of signal plots, and (2) outline the way in which this procedure can be used to implement an offline P300-based BCI Speller application. Its validity is verified by offline processing two datasets, one of data from ALS patients and another one from data of healthy subjects.

This article unfolds as follows: Section 2.1 is dedicated to explain the Feature Extraction method based on Histogram of Gradient Orientations of the Signal Plot: Section 2.1.1 shows the preprocessing pipeline, Section 2.1.3 describes the image generation of the signal plot, Section 2.1.4 presents the feature extraction procedure while Section 2.1.5 introduces the Speller Matrix Letter Identification procedure. In Section 2.2, the experimental protocol is expounded. Section 3 shows the results of applying the proposed technique. In the final Section 4 we expose our remarks, conclusions and future work.

## 2 MATERIALS AND METHODS

70 The P300 (Farwell and Donchin, 1988; Knuth et al., 2006) is a positive deflection of the EEG signal which  
71 occurs around 300 ms after the onset of a rare and deviant stimulus that the subject is expected to attend. It  
72 is produced under the oddball paradigm (Wolpaw and E., 2012) and it is consistent across different subjects.  
73 It has a lower amplitude ( $\pm 5\mu V$ ) compared to basal EEG activity, reaching a Signal to Noise Ratio (SNR)  
74 of around  $-15$  db estimated based on the amplitude of the P300 response signal divided by the standard  
75 deviation of the background EEG activity (Hu et al., 2010). This signal can be used to implement a speller  
76 application by means of a Speller Matrix (Farwell and Donchin, 1988). Fig. 1 shows an example of the  
77 Speller Matrix used in the OpenVibe open source software (Renard et al., 2010), where the flashes of rows  
78 and columns provide the deviant stimulus required to elicit this physiological response. Each time a row or  
79 a column that contains the desired letter flashes, the corresponding synchronized EEG signal should also  
80 contain the P300 signature and by detecting it, the selected letter can be identified.

81 **2.1 Feature Extraction from Signal Plots**

82 In this section, the signal preprocessing, the method for generating images from signal plots, the feature  
83 extraction procedure and the Speller Matrix identification are described.

84 **2.1.1 Preprocessing Pipeline**

85 The data obtained by the capturing device is digitalized and a multichannel EEG signal is constructed,  
86 where rows are sample points and columns are channels (electrodes).

- 87 • **Signal Enhancement:** The preprocessing stage consists of the enhancement of the SNR of the P300  
88 pattern above the level of basal EEG. The pipeline starts by applying a notch filter to the raw digital  
89 signal, a 4th degree 10 Hz lowpass Butterworth filter and finally a decimation with a Finite Impulse  
90 Response (FIR) filter of order 30 from the original sampling frequency down to 16 Hz(Krusienski  
91 et al., 2006).
- 92 • **Artifact Removal:** The multichannel EEG signal is processed on a channel by channel basis. For  
93 every complete sequence of 12 intensification of 6 rows and 6 columns, a basic artifact elimination  
94 procedure is implemented by removing the entire sequence when any signal deviates above/bellow  
95  $\pm 70\mu V$ .
- 96 • **Segmentation:** For each of the 12 intensifications, a window of  $t_{max} = 1$  second of the multichannel  
97 signal is extracted, starting from the stimulus onset, corresponding to each row/column intensification.  
98 Two of these segments should contain the P300 ERP signature time-locked to the flashing stimulus,  
99 one for the row, and one for the column.
- 100 • **Signal Averaging:** The P300 ERP is deeply buried under background EEG so the traditional approach  
101 to identify it is by point-to-point averaging the time-locked stacked signal segments. Hence the values  
102 which are not related to, and not time-locked to the onset of the stimulus are canceled out (Liang and  
103 Bougrain, 2008).

104 This last step determines the operation of any P300 Speller. In order to obtain an improved signal in  
105 terms of its SNR, repetitions of the sequence of row/column intensification are necessary. And, at the same  
106 time, as long as more repetitions are needed, the ability to transfer information faster is diminished, so  
107 there is a trade-off that must be acutely determined.

## 108 2.1.2 Ensemble Average

109 The procedure to obtain the point-to-point averaged signal goes as follows:

- 110 1. Highlight randomly the rows and columns from the matrix. There is one row and one column that  
111 should match the letter selected by the subject.
- 112 2. Repeat step 1  $k_a$  times, obtaining the single trial segments  $S_1(n, c), \dots, S_{k_a}(n, c)$ , of the EEG signal  
113 where the variables  $n \in \{1, \dots, n_{max}\}$  and  $c \in \{1, 2, \dots, Ch\}$  correspond to sample points and  
114 channel, respectively. The parameter  $Ch$  is the number of available EEG channels whereas  $n_{max} =$   
115  $F_s \cdot t_{max}$  is the segment length and  $F_s$  is the sampling frequency. The parameter  $k_a$  is the number of  
116 repetitions of intensifications and it is an input parameter of the algorithm.
- 117 3. Compute the Ensemble Average by

$$x(n, c) = \frac{1}{k_a} \sum_{i=1}^{k_a} S_i(n, c), n \in \{1, \dots, n_{max}\}, c \in \{1, \dots, Ch\} \quad (1)$$

118 for each row and column on the Speller Matrix.

## 119 2.1.3 Signal Plotting

120 Averaged signal segments are standardized and scaled by

$$\tilde{x}(n, c) = \left[ \gamma \cdot \frac{(x(n, c) - \bar{x}(c))}{\hat{\sigma}(c)} \right], n \in \{1, \dots, n_{max}\}, c \in \{1, 2, \dots, Ch\} \quad (2)$$

where  $\gamma > 0$  is an input parameter of the algorithm and it is related to the image scale. In addition,  $x(n, c)$  is the point-to-point averaged multichannel EEG signal for the sample point  $n$  and for channel  $c$ . Lastly,

$$\bar{x}(c) = \frac{1}{n_{max}} \sum_{n=1}^{n_{max}} x(n, c)$$

and

$$\hat{\sigma}(c) = \left( \frac{1}{n_{max} - 1} \sum_{n=1}^{n_{max}} (x(n, c) - \bar{x}(c))^2 \right)^{\frac{1}{2}}$$

121 are the mean and estimated standard deviation of  $x(n, c), n \in \{1, \dots, n_{max}\}$ , for each channel  $c$ .

122 Consequently, the image is constructed by placing the sample points according to

$$I(z_1, z_2) = \begin{cases} 255 & \text{if } z_1 = \gamma \cdot n; z_2 = \tilde{x}(n, c) + z(c) \\ 0 & \text{otherwise} \end{cases} \quad (3)$$

123 where  $(z_1, z_2) \in \mathbb{N} \times \mathbb{N}$  iterate over the width (based on the length of the signal segment) and height (based  
124 on the peak-to-peak amplitude) of the newly created image,  $n \in \{1, \dots, n_{max}\}$  and  $c \in \{1, 2, \dots, Ch\}$ .  
125 The values  $z(c), c \in \{1, 2, \dots, Ch\}$  are the location on the image where the signal's zero value has to be  
126 located in order to fit the entire signal within the image for each  $c$ :

$$z(c) = \left\lfloor \frac{\max_n \tilde{x}(n, c) - \min_n \tilde{x}(n, c)}{2} \right\rfloor - \left\lfloor \frac{\max_n \tilde{x}(n, c) + \min_n \tilde{x}(n, c)}{2} \right\rfloor \quad (4)$$

127 where the minimization and maximization are carried out for  $n$  varying between  $1 \leq n \leq n_{max}$ .

128 In order to complete the plot from the pixels, the Bresenham (Bresenham, 1965; Ramele et al., 2016)  
129 algorithm is used to interpolate straight lines between each pair of consecutive pixels.

### 130 2.1.4 Feature Extraction: Histogram of Gradient Orientations

131 On the generated image  $I$ , a keypoint  $\mathbf{kp}$  is placed on a pixel  $(x_{kp}, y_{kp})$  over the image plot and a window  
132 around the keypoint is considered. A local image patch of size  $S_p \times S_p$  pixels is constructed by dividing the  
133 window in 16 blocks of size  $3s$  each one, where  $s$  is the scale of the local patch and it is an input parameter  
134 of the algorithm. It is arranged in a  $4 \times 4$  grid and the pixel  $\mathbf{kp}$  is the patch center, thus  $S_p = 12s$  pixels.

135 A local representation of the signal shape within the patch can be described by obtaining the gradient  
136 orientations on each of the 16 blocks and creating a histogram of gradients. This technique is based on  
137 Lowe's SIFT (Lowe, 2004) method, and it is biomimetically inspired in how the visual cortex detects  
138 shapes by analyzing orientations (Edelman et al., 1997). In order to calculate the histogram, the interval  
139  $[0 - 360]$  of possible angles is divided in 8 bins, each one at 45 degrees.

140 Hence, for each spacial bin  $i, j = \{0, 1, 2, 3\}$ , corresponding to the indexes of each block  $B_{i,j}$ , the  
141 orientations are accumulated in a 3-dimensional histogram  $h$  through the following equation:

$$h(\theta, i, j) = 3s \sum_{\mathbf{p}} w_{ang}(\angle J(\mathbf{p}) - \theta) w_{ij} \left( \frac{\mathbf{p} - \mathbf{kp}}{3s} \right) |J(\mathbf{p})| \quad (5)$$

142 where  $\mathbf{p}$  is a pixel from within the patch,  $\theta$  is the angle bin with  $\theta \in \{0, 45, 90, 135, 180, 225, 270, 315\}$ ,  
143  $|J(\mathbf{p})|$  is the norm of the gradient vector in the pixel  $\mathbf{p}$  and it is computed using finite differences and  $\angle J(\mathbf{p})$   
144 is the angle of the gradient vector. The scalar  $w_{ang}(\cdot)$  and vector  $w_{ij}(\cdot)$  functions are linear interpolations  
145 used by Lowe (2004) and Vedaldi and Fulkerson (2010) to provide a weighting contribution to eight  
146 adjacent bins. They are calculated as

$$w_{ij}(\mathbf{v}) = w(v_x - x_i)w(v_y - y_i) \quad (6)$$

$$w_{ang}(\alpha) = \sum_k w\left(\frac{8\alpha}{2\pi} + 8r\right) \quad (7)$$

147 where  $x_i$  and  $y_i$  are the spatial bin centers located in  $x_i, y_i = \{-\frac{3}{2}, -\frac{1}{2}, \frac{1}{2}, \frac{3}{2}\}$ ,  $\mathbf{v} = (v_x, v_y)$  is a dummy  
148 vector variable and  $\alpha$  a dummy scalar variable. On the other hand,  $r$  is an integer that can vary freely which  
149 allows the argument  $\alpha$  to be unconstrained in terms of its values in radians. The interpolating function  $w(\cdot)$   
150 is defined as:

$$w(z) = \max(0, |z| - 1) \quad (8)$$

151 These binning functions conform a trilinear interpolation that has a combined effect of sharing the  
 152 contribution of each oriented gradient between their eight adjacent bins in a tridimensional cube in the  
 153 histogram space, and zero everywhere else.

154 Lastly, the fixed value of 3 is a magnification factor which corresponds to the number of pixels per each  
 155 block when  $s = 1$ . As the patch has 16 blocks and 8 bin angles are considered, a feature called *descriptor*  
 156 of 128 dimension is obtained.

157 Fig. 2 shows an example of a patch and a scheme of the histogram computation. In (A) a plot of the  
 158 signal and the patch centered around the keypoint is shown. In (B) the possible orientations on each patch  
 159 are illustrated. Only the upper-left four blocks are visible. The first eight orientations of the first block, are  
 160 labeled from 1 to 8 clockwise. The orientations of the second block  $B_{1,2}$  are labeled from 9 to 16. This  
 161 labeling continues left-to-right, up-down until the eight orientations for all the sixteen blocks are assigned.  
 162 They form the corresponding kp-descriptor of 128 coordinates. Finally, in (C) an enlarged image plot is  
 163 shown where the oriented gradient vector for each pixel can be seen.

#### 164 2.1.5 Speller Matrix letter Identification

165 The aim is to identify the selected letter from the matrix. Previously, during the training phase, two  
 166 descriptors are extracted from averaged signal segments which correspond to the letter where the user was  
 167 supposed to be focusing onto. These descriptors are the P300 templates which are grouped in a template  
 168 set called  $T$ . This set is constructed using the steps described in Section 2.1.2 and the steps A and B of  
 169 the following algorithm. Segments corresponding to rows are labeled 1-6, whereas those corresponding to  
 170 columns are labeled 7-12. The whole process has the following steps:

171 First highlight randomly the rows and columns from the matrix and obtain the Ensemble Average as  
 172 detailed in steps 1, 2 and 3 in Section 2.1.2.

- 173 • **Step A:** Plot the signals  $x(n, c)$ ,  $n \in \{1, \dots, n_{max}\}$ ,  $c \in \{1, \dots, Ch\}$ , according Section 2.1.3 in  
 174 order to generate the images  $I_1^{row}, \dots, I_6^{row}$  and  $I_7^{col}, \dots, I_{12}^{col}$  for rows and columns, respectively.
- 175 • **Step B:** Obtain the descriptors  $d_1^{row}, \dots, d_6^{row}$  and  $d_7^{col}, \dots, d_{12}^{col}$  for rows and columns, respectively  
 176 from  $I_1^{row}, \dots, I_6^{row}$  and  $I_7^{col}, \dots, I_{12}^{col}$  in accordance to the method described in Section 2.1.4.
- 177 • **Step C:** Match to the Template  $T$  by computing

$$r\hat{o}w = \arg \min_{u \in \{1, \dots, 6\}} \sum_{q \in NN_T(d_u^{row})} \|q - d_u^{row}\|^2 \quad (9)$$

178 and

$$\hat{c}ol = \arg \min_{u \in \{7, \dots, 12\}} \sum_{q \in NN_T(d_u^{col})} \|q - d_u^{col}\|^2 \quad (10)$$

179 where  $NN_T(d_u^l)$ ,  $l \in \{row, col\}$  is the set of the  $k$  nearest neighbors to  $d_u^l$  and  $q$  is a template  
 180 descriptor that belongs to it. This set is obtained by sorting all the elements in  $T$  based on the distances  
 181 between them and  $d_u^l$ , choosing the  $k$  smaller elements. This procedure is a modification of the  
 182 k-NBNN algorithm (Boiman et al., 2008).

183 By computing the aforementioned equations, the letter of the matrix can be determined from the intersection  
 184 of the row  $r\hat{o}w$  and column  $\hat{c}ol$ . Figure 3 shows a scheme of this process.

---

**185 2.2 Experimental Protocol**

186 To verify the validity of the proposed framework and method, the public dataset 008-2014 (Riccio et al.,  
187 2013) published on the BNCI-Horizon website (Brunner et al., 2014) by IRCCS Fondazione Santa Lucia,  
188 is used. Additionally, an own dataset with the same experimental conditions is generated. Both of them are  
189 utilized to perform an offline BCI Simulation to decode the spelled words from the provided signals.

190 The algorithm is implemented using VLFeat (Vedaldi and Fulkerson, 2010) Computer Vision libraries on  
191 MATLAB V2014a (Mathworks Inc., Natick, MA, USA).

192 In the following sections the characteristics of the datasets and parameters of the identification algorithm  
193 are described.

**194 2.2.1 P300 ALS Public Dataset**

195 The experimental protocol used to generate this dataset is explained in (Riccio et al., 2013) but can  
196 be summarized as follows: 8 subjects with confirmed diagnoses but on different stages of ALS disease,  
197 were recruited and accepted to perform the experiments. The Visual P300 detection task designed for this  
198 experiment consisted of spelling 7 words of 5 letters each, using the traditional P300 Speller Matrix (Farwell  
199 and Donchin, 1988). The flashing of rows and columns provide the deviant stimulus required to elicit this  
200 physiological response. The first 3 words are used for training and the remaining 4 words, for testing with  
201 visual feedback. A trial, as defined by the BCI2000 platform (Schalk et al., 2004), is every attempt to select  
202 a letter from the speller. It is composed of signal segments corresponding to  $k_a = 10$  repetitions of flashes  
203 of 6 rows and  $k_a = 10$  repetitions of flashes of 6 columns of the matrix, yielding 120 repetitions. Flashing  
204 of a row or a column is performed for 0.125 s, following by a resting period (i.e. inter-stimulus interval) of  
205 the same length. After 120 repetitions an inter-trial pause is included before resuming with the following  
206 letter.

207 The recorded dataset was sampled at 256 Hz and it consisted of a scalp multichannel EEG signal for  
208 electrode channels Fz, Cz, Pz, Oz, P3, P4, PO7 and PO8, identified according to the 10-20 International  
209 System, for each one of the 8 subjects. The recording device was a research-oriented digital EEG device  
210 (g.Mobilab, g.Tec, Austria) and the data acquisition and stimuli delivery were handled by the BCI2000  
211 open source software (Schalk et al., 2004).

212 In order to assess and verify the identification of the P300 response, subjects are instructed to perform a  
213 copy-spelling task. They have to fix their attention to successive letters for copying a previously determined  
214 set of words, in contrast to a free-running operation of the speller where each user decides on its own what  
215 letter to choose.

**216 2.2.2 P300 for healthy subjects**

217 We replicate the same experiment on healthy subjects (Ramele et al., 2017) using a wireless digital EEG  
218 device (g.Nautilus, g.Tec, Austria). The experimental conditions are the same as those used for the previous  
219 dataset, as detailed in section 2.2.1.

220 Participants are recruited voluntarily and the experiment is conducted anonymously in accordance with  
221 the declaration of Helsinki published by the World Health Organization. No monetary compensation is  
222 handed out and all participants agree and sign a written informed consent. All healthy subjects have normal  
223 or corrected-to-normal vision and no history of neurological disorders. The experiment is performed with 8  
224 subjects, 6 males, 2 females, 6 right-handed, 2 left-handed, average age 29.00 years, standard deviation  
225 11.56 years, range 20-56 years.

226 EEG data is collected in a single recording session. Participants are seated in a comfortable chair, with  
 227 their vision aligned to a computer screen located one meter in front of them. The handling and processing  
 228 of the data and stimuli is conducted by the OpenVibe platform (Renard et al., 2010).

229 Gel-based active electrodes (g.LADYbird, g.Tec, Austria) are used on the same locations Fz, Cz, Pz,  
 230 Oz, P3,P4, PO7 and PO8. Reference is set to the right ear lobe and ground is preset as the AFz position.  
 231 Sampling frequency is slightly different, and is set to 250 Hz, which is the closest possible to the one used  
 232 with the other dataset.

### 233 2.2.3 Parameters

234 The patch size is  $S_P = 12s \times 12s$  pixels, where  $s$  is the scale of the local patch and it is an input parameter  
 235 of the algorithm. The P300 event can have a span of 400 ms and its amplitude can reach  $10\mu V$  (Rao,  
 236 2013). Hence it is necessary to utilize a size patch  $S_P$  that could capture an entire transient event. With this  
 237 purpose in consideration, the  $s$  value election is essential.

238 We propose the Equations 11 and 12 to compute the scale value in horizontal and vertical directions,  
 239 respectively.

$$s_x = \frac{\lambda \cdot Fs}{12} \cdot \gamma \quad (11)$$

$$s_y = \frac{\Delta\mu V}{12} \cdot \gamma \quad (12)$$

240 where  $\lambda$  is the length in seconds covered by the patch,  $Fs$  is the sampling frequency of the EEG signal  
 241 (downsampled to 16 Hz) and  $\Delta\mu V$  corresponds to the amplitude in microvolts that can be covered by the  
 242 height of the patch. The geometric structure of the patch forces a squared configuration, then we discerned  
 243 that by using  $s = s_x = s_y = 3$  and  $\gamma = 4$ , the local patch and the descriptor can identify events of  $9\mu V$   
 244 of amplitude, with a span of  $\lambda = 0.56$  seconds. This also determines that 1 pixel represents  $\frac{1}{\gamma} = \frac{1}{4}\mu V$  on  
 245 the vertical direction and  $\frac{1}{Fs \cdot \gamma} = \frac{1}{64}$  seconds on the horizontal direction. Descriptors  $kp$  are located at  
 246  $(x_{kp}, y_{kp}) = (0.55Fs \cdot \gamma, z(c)) = (35, z(c))$  for the corresponding channel  $c$  (see Eq. 4). In this way the  
 247 whole transient event is captured. Figure 4 shows a patch of a signal plot covering the complete amplitude  
 248 (vertical direction) and the complete span of the signal event (horizontal direction).

249 Lastly, the number of channels  $Ch$  is equal to 8 for both datasets, and the number of intensification  
 250 sequences  $k_a$  is statically assigned to 10. The parameter  $k$  used to construct the set  $NN_T(d_u^l)$ ,  $l \in$   
 251  $\{row, col\}$  is assigned to  $k = 7$ , which was found empirically to achieve better results. In addition, the  
 252 norm used on Equations 9 and 10 is the cosine norm, and descriptors are normalized to  $[-1, 1]$ .

## 3 RESULTS

253 Table 1 shows the results of applying the algorithm to the subjects of the public dataset of ALS patients.  
 254 The percentage of correctly spelled letters is calculated while performing an offline BCI Simulation. From  
 255 the seven words for each subject, the first three are used as training, and the remaining four for testing.  
 256 The best performing channel is informed as well. The chance level is 2%. It can be observed that the best  
 257 performance of the letter identification method is reached in various channels depending on the subject  
 258 been studied.

259 The Information Transfer Rate (ITR), or Bit Transfer Rate (BTR), in the case of reactive BCIs (Wolpaw  
260 and E., 2012) depends on the amount of signal averaging required to transmit a valid and robust selection.  
261 Fig. 5 shows the performance curves for varying intensification sequences. It can be noticed that the  
262 percentage of correctly identified letters depends on the number of intensification sequences  $k_a$  that are  
263 used to obtain the averaged signal. Moreover, when the number of intensification sequences tend to 1,  
264 which corresponds to single-trial letter identification, the performance is reduced. As mentioned before, the  
265 SNR of the single-trial P300 is very low and the shape of its P300 component is not very well defined.

266 In Table 2 results obtained for 8 healthy subjects are shown. The obtained performance were slightly  
267 inferior than those obtained for ALS patients but well above chance level.

268 The P300 ERP consists of two overlapping components: the P3a and P3b, the former with frontocentral  
269 distribution while the later stronger on centroparietal region (Polich, 2007). Hence, the standard practice is  
270 to find the stronger response on the central channel Cz (Riccio et al., 2013). However, Krusienski et al.  
271 (2006) show that the response may also arise in occipital regions. We found that by analyzing only the  
272 waveforms, occipital channels PO8 and PO7 show higher performances for some subjects.

273 As subjects have varying *latencies* and *amplitudes* of their P300 components, they also have a varying  
274 stability of the *shape* of the generated ERP (Nam et al., 2010). Figure 6 shows the P300 templates patches  
275 for patients 8 and 3 from the dataset of ALS patients. It can be discerned that in coincidence with the  
276 performance results, the P300 signature is more clear and consistent for subject 8 (A) while for subject 3  
277 (B) the characteristic pattern is more difficult to perceive.

278 Additionally, the stability of the P300 component waveform has been extensively studied in patients  
279 with ALS (Eric W. Sellers and Emanuel Donchin, 2006; Madarame et al., 2008; Nijboer and Broermann,  
280 2009; Mak et al., 2012; McCane et al., 2015) where it was found that these patients have a stable P300  
281 component, which were also sustained across different sessions. In line with these results we do not find  
282 evidence of a difference in terms of the performance obtained for the group of patients with ALS and the  
283 healthy group of volunteers. Particularly, the best performance is obtained for a subject from the ALS  
284 dataset for which, based on visual observation, the shape of they P300 component is consistently identified.

285 It is important to remark that when applied to binary images obtained from signal plots, the feature  
286 extraction method described in Section 2.1.4 generates sparse descriptors. Under this subspace we found  
287 that using the cosine metric yielded a significant performance improvement. On the other hand, the unary  
288 classification scheme based on the NBNN algorithm proved very beneficial for the P300 Speller Matrix.  
289 This is due to the fact that this approach solves the unbalance dataset problem which is inherent to the  
290 oddball paradigm (Tibon and Levy, 2015).

## 4 DISCUSSION

291 Among other applications of Brain Computer Interfaces, the goal of the discipline is to provide  
292 communication assistance to people affected by neuro-degenerative diseases, who are the most likely  
293 population to benefit from BCI systems and EEG processing and analysis.

294 In this work, a method to detect transient P300 components from EEG signals based on their waveform  
295 characterization in digital time-space, is presented. Additionally, its validity is evaluated using a public  
296 dataset of ALS patients and an own dataset of healthy subjects.

297 This method has the advantage that shapes of waveforms can be analyzed in an objective way. We  
298 observed that the shape of the P300 component is more stable in occipital channels, where the performance

299 for identifying letters is higher. We additionally verified that ALS P300 signatures are stable in comparison  
300 to those of healthy subjects. Further work should be conducted over larger samples to cross-check the  
301 validity of these results.

302 We believe that the use of descriptors based on histogram of gradient orientation, presented in this work,  
303 can also be utilized for deriving a shape metric in the space of the P300 signals which can complement  
304 other metrics based on time-domain as those defined by Mak et al. (2012). It is important to notice that the  
305 analysis of waveform shapes is usually performed in a qualitative approach based on visual inspection (Eric  
306 W. Sellers and Emanuel Donchin, 2006).

307 The goal of this work is to answer the question if a P300 component could be solely determined by  
308 inspecting automatically their waveforms. We conclude affirmatively, though two very important issues  
309 still remain:

310 First, the stability of the P300 in terms of its shape is crucial: the averaging procedure, montages, the  
311 signal to noise ratio and spatial filters all of them are non-physiological factors that affect the stability of  
312 the shape of the P300 ERP. We tested a preliminary approach to assess if the morphological shape of the  
313 P300 can be stabilized by applying different latency shifts to segments and we verified that there is a better  
314 performance when a correct single-trial alignment is applied. We also applied Dynamic Time Warping  
315 (DTW) (Casarotto et al., 2005) but we were unable to find a substantial improvement. Further work to  
316 study the stability of the P300 signature component needs to be addressed.

317 The second problem is the amplitude variation of the P300. We propose a solution by standardizing the  
318 signal, shown in Eq. 2. It has the effect of normalizing the peak-to-peak amplitude, moderating its variation.  
319 It has also the advantage of reducing noise that was not reduced by the averaging procedure. It is important  
320 to remark that the signal variance depends on the number of single-trials segments used to compute it (Van  
321 Drongelen, 2006). The standardizing process converts the signal to unit signal variance which makes it  
322 independent of the number  $k_a$  of signals averaged. Although this is initially an advantageous approach, the  
323 standardizing process reduces the amplitude of any significant P300 complex diminishing its automatic  
324 interpretation capability.

325 In our opinion, the best benefit of the presented method is that a closer collaboration with physicians can  
326 be fostered, since this procedure intent to imitate human visual observation. Automatic classification of  
327 patterns in EEG that are specifically identified by their shapes like K-Complex, Vertex Waves, Positive  
328 Occipital Sharp Transient (Hartman, 2005) are a prospect future work to be considered. We are currently  
329 working in unpublished material analyzing KComplex that could eventually provide assistance to physicians  
330 to locate these EEG patterns, specially in long recording periods, frequent in sleep research. Additionally,  
331 it can be used for artifact removal which is performed on many occasions by visually inspecting signals.  
332 This is due to the fact that the descriptors are a direct representation of the shape of signal waveforms. In  
333 line with these applications, it can be used to build a database (Chavarriaga et al., 2017) of quantitative  
334 representations of waveforms and improve atlases (Hartman, 2005), which are currently based on qualitative  
335 descriptions of signal shapes.

## CONFLICT OF INTEREST STATEMENT

336 The authors declare that the research was conducted in the absence of any commercial or financial  
337 relationships that could be construed as a potential conflict of interest.

## AUTHOR CONTRIBUTIONS

338 This work is part of the PhD thesis of RR which is directed by JS and codirected by AV.

## FUNDING

339 This project was supported by the ITBACyT-15 funding program issued by ITBA University from Buenos  
340 Aires, Argentina.

## REFERENCES

- 341 Alvarado-González, M., Garduño, E., Bribiesca, E., Yáñez-Suárez, O., and Medina-Bañuelos, V. (2016).  
342 P300 Detection Based on EEG Shape Features. *Computational and Mathematical Methods in Medicine*,  
343 1–14doi:10.1155/2016/2029791
- 344 Berger, S., Schneider, G., Kochs, E., and Jordan, D. (2017). Permutation Entropy: Too Complex a Measure  
345 for EEG Time Series? *Entropy* 2017, Vol. 19, Page 692 19, 692. doi:10.3390/E19120692
- 346 Boiman, O., Shechtman, E., and Irani, M. (2008). In defense of nearest-neighbor based image classification.  
347 *26th IEEE Conference on Computer Vision and Pattern Recognition, CVPR* doi:10.1109/CVPR.2008.  
348 4587598
- 349 Bresenham, J. E. (1965). Algorithm for computer control of a digital plotter. *IBM Systems Journal* 4,  
350 25–30
- 351 Brunner, C., Blankertz, B., Cincotti, F., Kübler, A., Mattia, D., Miralles, F., et al. (2014). BNCI Horizon  
352 2020 – Towards a Roadmap for Brain / Neural Computer Interaction. *Lecture Notes in Computer Science*  
353 8513, 475–486
- 354 Carlson, T. and del R. Millan, J. (2013). Brain-controlled wheelchairs: A robotic architecture. *IEEE  
355 Robotics & Automation Magazine* 20, 65–73. doi:10.1109/MRA.2012.2229936
- 356 Casarotto, S., Bianchi, A., Cerutti, S., and Chiarenza, G. (2005). Dynamic time warping in the analysis of  
357 event-related potentials. *IEEE Engineering in Medicine and Biology Magazine* 24, 68–77. doi:10.1109/  
358 MEMB.2005.1384103
- 359 Chavarriaga, R., Fried-Oken, M., Kleih, S., Lotte, F., and Scherer, R. (2017). Heading for new shores!  
360 Overcoming pitfalls in BCI design. *Brain-Computer Interfaces* 4, 60–73. doi:10.1080/2326263X.2016.  
361 1263916
- 362 Clerc, M., Bougrain, L., and Lotte, F. (2016). *Brain-computer interfaces, Technology and applications*  
363 2(Cognitive Science) (ISTE Ltd. and Wiley)
- 364 De Vos, M. and Debener, S. (2014). Mobile EEG: Towards brain activity monitoring during natural action  
365 and cognition. *International Journal of Psychophysiology* 91, 1–2. doi:10.1016/j.ijpsycho.2013.10.008
- 366 Edelman, S., Intrator, N., and Poggio, T. (1997). Complex cells and object recognition
- 367 Eric W. Sellers and Emanuel Donchin, A. K. (2006). Brain?Computer Interface Research at the University  
368 of South Florida Cognitive Psychophysiology Laboratory:The P300 Speller , 221–224doi:10.1109/  
369 TNSRE.2006.875580
- 370 Farwell, L. A. and Donchin, E. (1988). Talking off the top of your head: toward a mental prosthesis utilizing  
371 event-related brain potentials. *Electroencephalography and clinical neurophysiology* 70, 510–23
- 372 Guger, C., Allison, B. Z., and Lebedev, M. A. (2017). Introduction. In *Brain Computer Interface Research:  
373 A State of the Art Summary* 6 (Springer, Cham). 1–8. doi:10.1007/978-3-319-64373-1\_1

- 374 Guger, C., Daban, S., Sellers, E., Holzner, C., Krausz, G., Carabalona, R., et al. (2009). How many people  
375 are able to control a P300-based brain-computer interface (BCI)? *Neuroscience Letters* 462, 94–98.  
376 doi:10.1016/j.neulet.2009.06.045
- 377 Hartman, a. L. (2005). *Atlas of EEG Patterns*, vol. 65 (Lippincott Williams & Wilkins). doi:10.1212/01.  
378 wnl.0000174180.41994.39
- 379 Hu, L., Mouraux, A., Hu, Y., and Iannetti, G. D. (2010). A novel approach for enhancing the signal-to-noise  
380 ratio and detecting automatically event-related potentials (ERPs) in single trials. *NeuroImage* 50, 99–111.  
381 doi:10.1016/j.neuroimage.2009.12.010
- 382 Huggins, J. E., Alcaide-Aguirre, R. E., and Hill, K. (2016). Effects of text generation on P300 brain-  
383 computer interface performance. *Brain-Computer Interfaces* 3, 112–120. doi:10.1080/2326263X.2016.  
384 1203629
- 385 Jure, F., Carrere, L., Gentiletti, G., and Tabernig, C. (2016). BCI-FES system for neuro-rehabilitation of  
386 stroke patients. *Journal of Physics: Conference Series* 705, 1–8. doi:10.1088/1742-6596/705/1/012058
- 387 Knuth, K. H., Shah, A. S., Truccolo, W. A., Ding, M., Bressler, S. L., and Schroeder, C. E. (2006).  
388 Differentially variable component analysis: Identifying multiple evoked components using trial-to-trial  
389 variability. *Journal of Neurophysiology* 95, 3257–3276. doi:10.1152/jn.00663.2005
- 390 Krusienski, D. J., Sellers, E. W., Cabestaing, F., Bayoudh, S., McFarland, D. J., Vaughan, T. M., et al.  
391 (2006). A comparison of classification techniques for the P300 Speller. *Journal of Neural Engineering*  
392 3, 299–305. doi:10.1088/1741-2560/3/4/007
- 393 Liang, N. and Bougrain, L. (2008). Averaging techniques for single-trial analysis of oddball event-related  
394 potentials. *4th International Brain-Computer* , 1–6
- 395 Lotte, F., Faller, J., Guger, C., Renard, Y., Pfurtscheller, G., Lécuyer, A., et al. (2013). *Combining BCI*  
396 *with Virtual Reality: Towards New Applications and Improved BCI* (Berlin, Heidelberg: Springer Berlin  
397 Heidelberg). 197–220. doi:10.1007/978-3-642-29746-5\_10
- 398 Lowe, G. (2004). SIFT - The Scale Invariant Feature Transform. *International Journal* 2, 91–110
- 399 Madarame, T., Tanaka, H., Inoue, T., Kamata, M., and Shino, M. (2008). The development of a brain  
400 computer interface device for amyotrophic lateral sclerosis patients. In *Conference Proceedings - IEEE*  
401 *International Conference on Systems, Man and Cybernetics* (IEEE), 2401–2406. doi:10.1109/ICSMC.  
402 2008.4811654
- 403 Mak, J. N., McFarland, D. J., Vaughan, T. M., McCane, L. M., Tsui, P. Z., Zeitlin, D. J., et al. (2012). EEG  
404 correlates of P300-based brain-computer interface (BCI) performance in people with amyotrophic lateral  
405 sclerosis. *Journal of Neural Engineering* 9. doi:10.1088/1741-2560/9/2/026014
- 406 McCane, L. M., Heckman, S. M., McFarland, D. J., Townsend, G., Mak, J. N., Sellers, E. W., et al.  
407 (2015). P300-based brain-computer interface (BCI) event-related potentials (ERPs): People with  
408 amyotrophic lateral sclerosis (ALS) vs. age-matched controls. *Clinical Neurophysiology* 126, 2124–2131.  
409 doi:10.1016/j.clinph.2015.01.013
- 410 Nam, C. S., Li, Y., and Johnson, S. (2010). Evaluation of P300-based brain-computer interface in real-  
411 world contexts. *International Journal of Human-Computer Interaction* 26, 621–637. doi:10.1080/  
412 10447311003781326
- 413 Nijboer, F. and Broermann, U. (2009). Brain Computer Interfaces for Communication and Control in  
414 Locked-in Patients. In *Graimann B., Pfurtscheller G., Allison B. (eds) Brain-Computer Interfaces. The*  
415 *Frontiers Collection*. (Springer Berlin Heidelberg). 185–201. doi:10.1007/978-3-642-02091-9\_11
- 416 Novak, D., Sigrist, R., Gerig, N. J., Wyss, D., Bauer, R., Gotz, U., et al. (2018). Benchmarking brain-  
417 computer interfaces outside the laboratory: The cybathlon 2016. *Frontiers in Neuroscience* 11, 756.  
418 doi:10.3389/fnins.2017.00756

- 419 Polich, J. (2007). Updating P300: An integrative theory of P3a and P3b. *Clinical Neurophysiology* 118,  
420 2128–2148. doi:10.1016/j.clinph.2007.04.019
- 421 Ramele, R., Villar, A. J., and Santos, J. M. (2016). BCI classification based on signal plots and SIFT  
422 descriptors. In *4th International Winter Conference on Brain-Computer Interface, BCI 2016* (Yongpyong:  
423 IEEE), 1–4. doi:10.1109/IWW-BCI.2016.7457454
- 424 [Dataset] Ramele, R., Villar, A. J., and Santos, J. M. (2017). P300-dataset rrid scr\_015977. <https://www.kaggle.com/rramele/p300samplingdataset>
- 426 Rao, R. P. N. (2013). *Brain-Computer Interfacing: An Introduction* (New York, NY, USA: Cambridge  
427 University Press)
- 428 Renard, Y., Lotte, F., Gibert, G., Congedo, M., Maby, E., Delannoy, V., et al. (2010). OpenViBE: An  
429 Open-Source Software Platform to Design, Test, and Use Brain–Computer Interfaces in Real and Virtual  
430 Environments. *Presence: Teleoperators and Virtual Environments* 19, 35–53. doi:10.1162/pres.19.1.35
- 431 Riccio, A., Simione, L., Schettini, F., Pizzimenti, A., Inghilleri, M., Belardinelli, M. O., et al. (2013).  
432 Attention and P300-based BCI performance in people with amyotrophic lateral sclerosis. *Frontiers in  
433 Human Neuroscience* 7, 732. doi:10.3389/fnhum.2013.00732
- 434 Riener, R. and Seward, L. J. (2014). Cybathlon 2016. *2014 IEEE International Conference on Systems,  
435 Man, and Cybernetics (SMC)*, 2792–2794doi:10.1109/SMC.2014.6974351
- 436 Schalk, G., McFarland, D. J., Hinterberger, T., Birbaumer, N., and Wolpaw, J. R. (2004). BCI2000: a  
437 general-purpose brain-computer interface (BCI) system. *IEEE transactions on bio-medical engineering*  
438 51, 1034–43. doi:10.1109/TBME.2004.827072
- 439 Schomer, D. L. and Silva, F. L. D. (2010). *Niedermeyer's Electroencephalography: Basic Principles,  
440 Clinical Applications, and Related Fields* (Walters Klutter -Lippincott Williams & Wilkins)
- 441 Tibon, R. and Levy, D. A. (2015). Striking a balance: analyzing unbalanced event-related potential data.  
442 *Frontiers in psychology* 6, 555. doi:10.3389/fpsyg.2015.00555
- 443 Van Drongelen, W. (2006). *Signal processing for neuroscientists: an introduction to the analysis of  
444 physiological signals* (Academic press)
- 445 Vedaldi, A. and Fulkerson, B. (2010). VLFeat - An open and portable library of computer vision algorithms.  
446 *Design* 3, 1–4. doi:10.1145/1873951.1874249
- 447 Wolpaw, J. and E., W. (2012). *Brain-Computer Interfaces: Principles and Practice* (Oxford University  
448 Press)
- 449 Yamaguchi, T., Fujio, M., Inoue, K., and Pfurtscheller, G. (2009). Design method of morphological  
450 structural function for pattern recognition of EEG signals during motor imagery and cognition. In *Fourth  
451 International Conference on Innovative Computing, Information and Control (ICICIC)*. 1558–1561.  
452 doi:10.1109/ICICIC.2009.161

**Table 1.** Percentage of correctly predicted letters while performing an offline BCI Simulation for the best performing channel for each subject of the public dataset of ALS patients. The spelled words are *GATTO*, *MENTE*, *VIOLA* and *REBUS*.

Participant	BPC	Performance
1	Cz	35%
2	Fz	85%
3	Cz	25%
4	PO8	55%
5	PO7	40%
6	PO7	60%
7	PO8	80%
8	PO7	95%

**Table 2.** Percentage of correctly predicted letters while performing an offline BCI Simulation for the best performing channel for each subject of the own dataset. The spelled words are *MANSO*, *CINCO*, *JUEGO* and *QUESO*.

Participant	BPC	Performance
1	Oz	40%
2	PO7	30%
3	P4	40%
4	P4	45%
5	P4	60%
6	Pz	50%
7	PO7	70%
8	P4	50%



**Figure 1.** Example of the  $6 \times 6$  Speller Matrix used in the study. Rows and columns flash intermittently in random permutations.

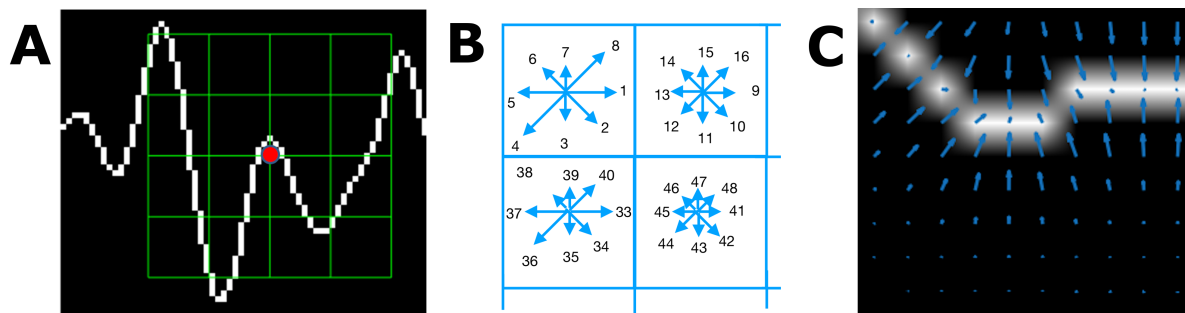


**Figure 2.** (A) Example of a plot of the signal, a keypoint and the corresponding patch. (B) A scheme of the orientation's histogram computation. Only the upper-left four blocks are visible. The first eight orientations of the first block, are labeled from 1 to 8 clockwise. The orientation of the second block  $B_{1,2}$  is labeled from 9 to 16. This labeling continues left-to-right, up-down until the eight orientations for all the sixteen blocks are assigned. They form the corresponding kp-descriptor of 128 coordinates. The length of each arrow represent the value of the histogram on each direction for each block. (C) Vector field of oriented gradients. Each pixel is assigned an orientation and magnitude calculated using finite differences.

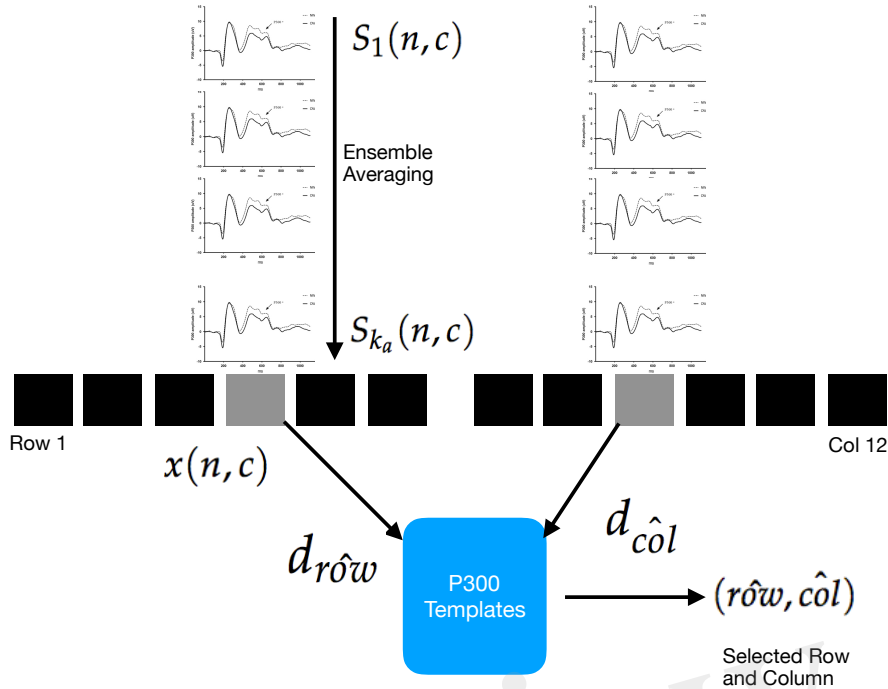


**Figure 3.** Single trial segments  $S_i$  are averaged for the 6 rows and 6 columns. From the averaged signal, the image of the signal plot is generated and each descriptor is computed. By comparing each descriptor against the set of templates, the P300 ERP can be detected, and finally the desired letter from the matrix can be inferred.

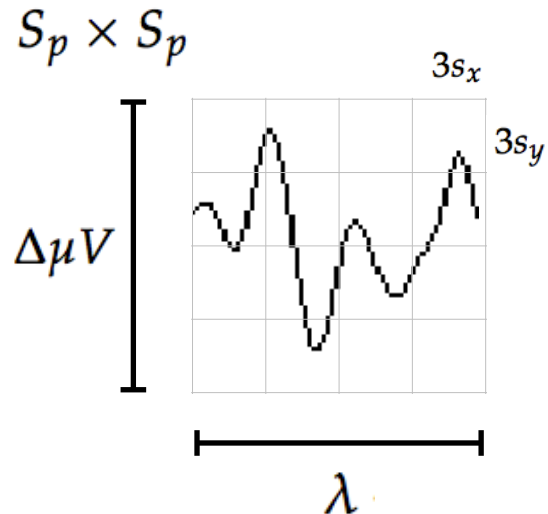


**Figure 4.** The scale of local patch is selected in order to capture the whole transient event. The size of the patch is  $S_p \times S_p$  pixels. The vertical size consists of 4 blocks of size  $3s_y$  pixels which is high enough as to contain the signal  $\Delta\mu V$ , the peak-to-peak amplitude of the transient event. The horizontal size includes 4 blocks of  $3s_x$  and covers the entire duration in seconds of the transient signal event,  $\lambda$ .

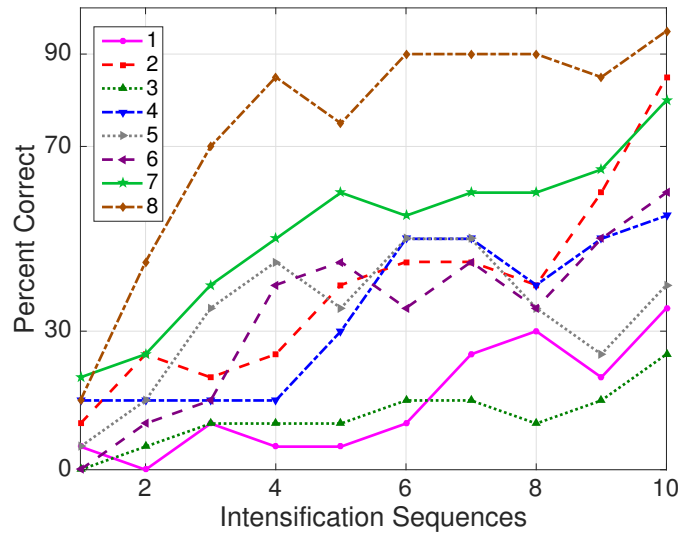


**Figure 5.** Performance curves for the eight subjects included in the dataset of ALS patients. Three out of eight subjects achieved the necessary performance to implement a valid P300 speller.

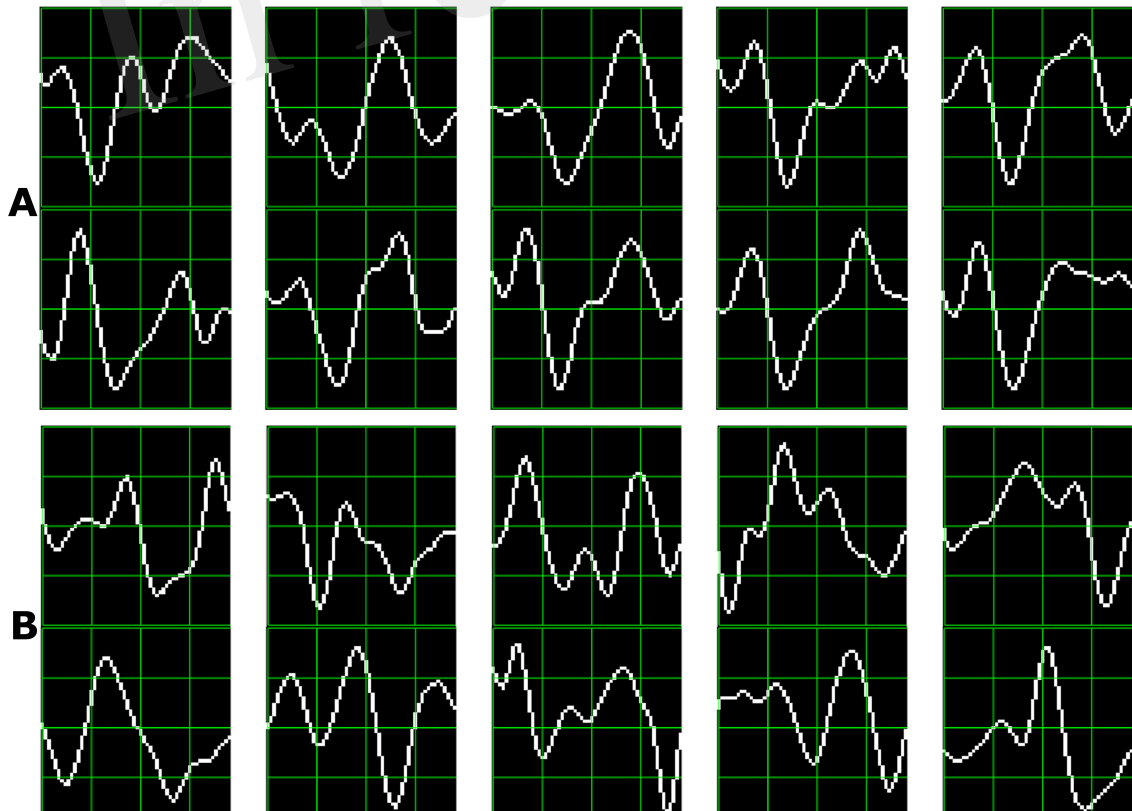


**Figure 6.** P300 template patches for subjects 8 (A) and 3 (B). As traditional done in neuroscience research, downward is positive polarity.

Figure 1.TIF

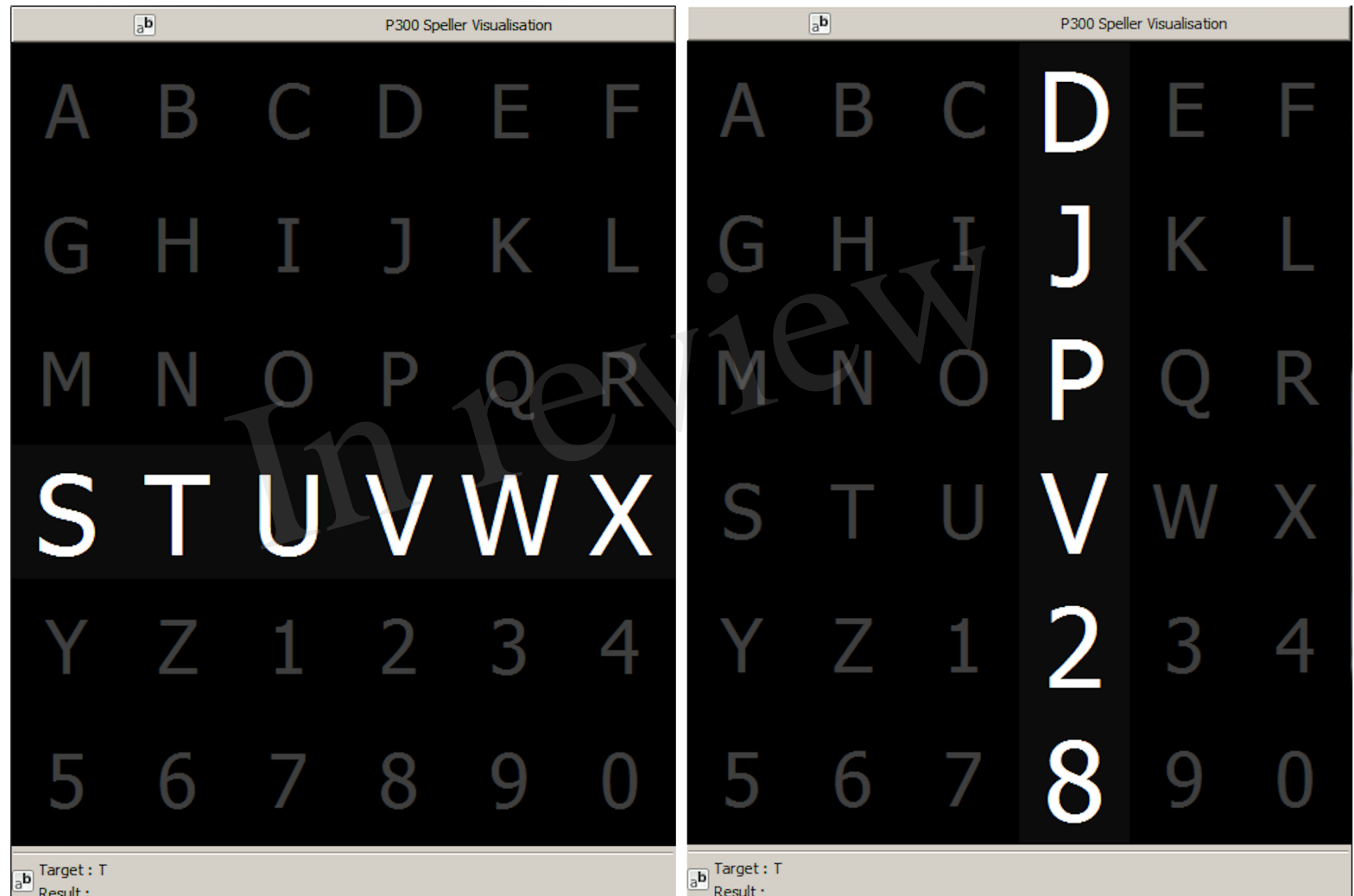


Figure 2.TIF

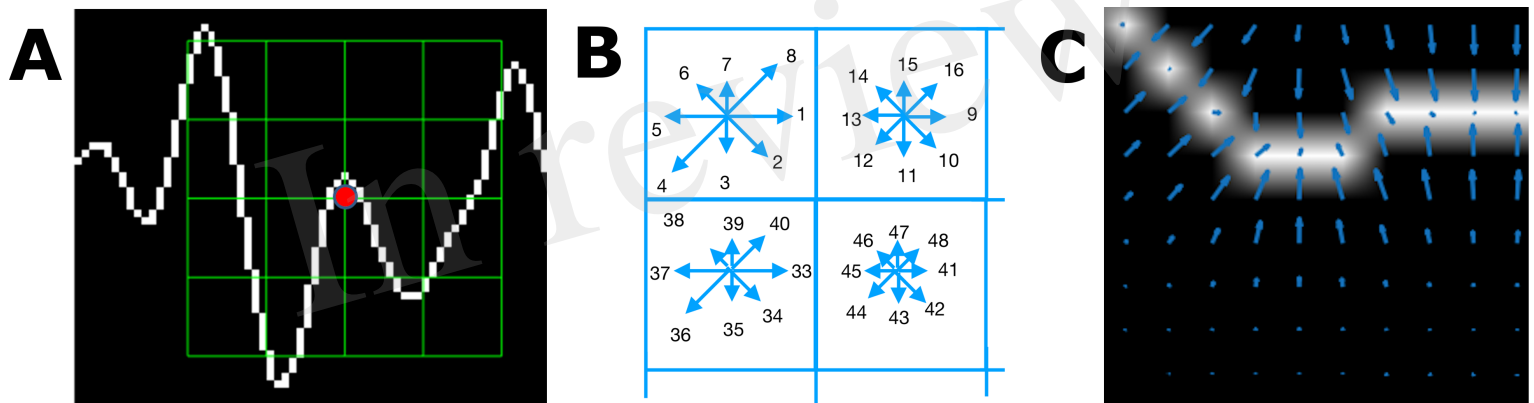


Figure 3.TIF

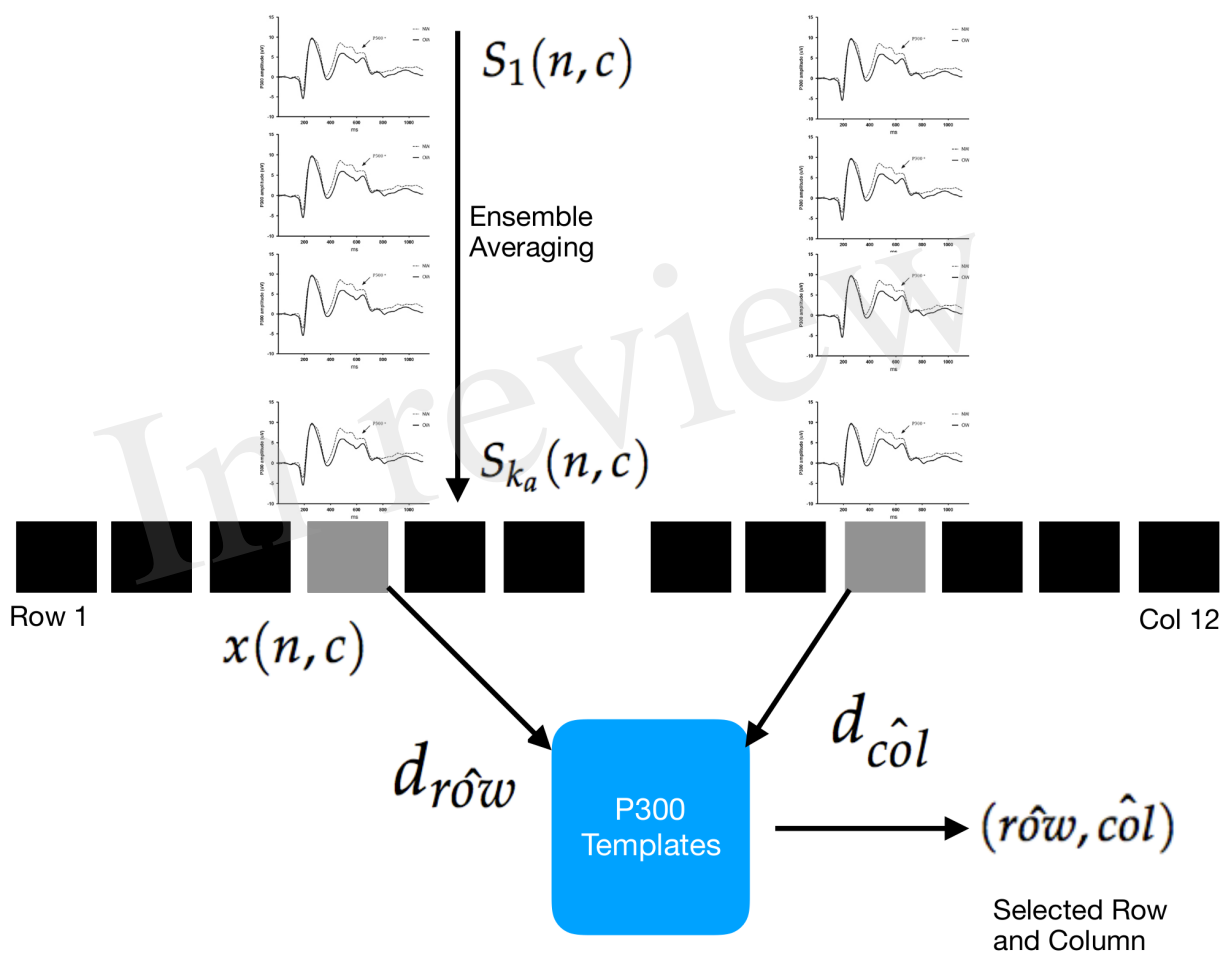


Figure 4.TIF

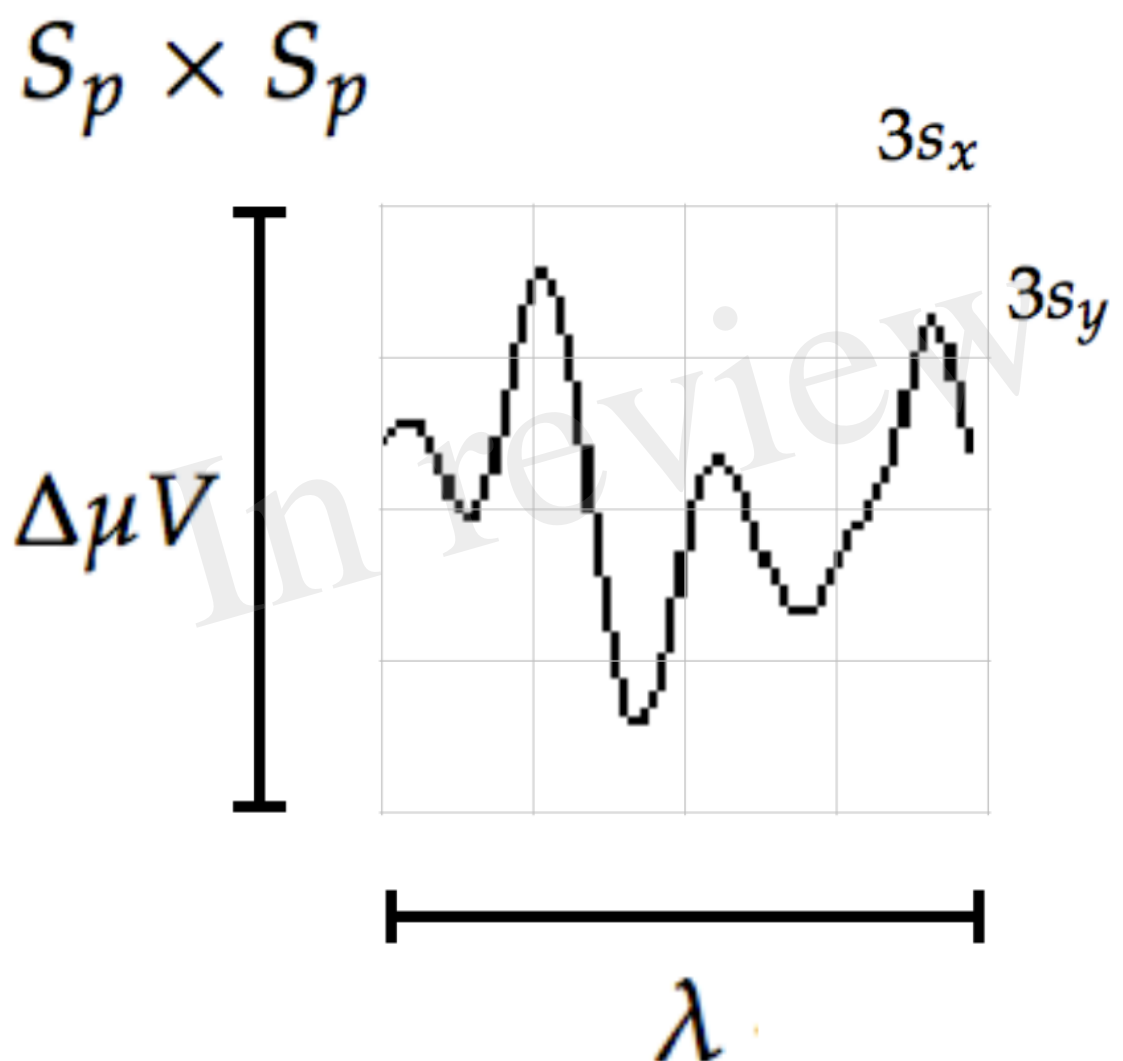


Figure 5.TIF

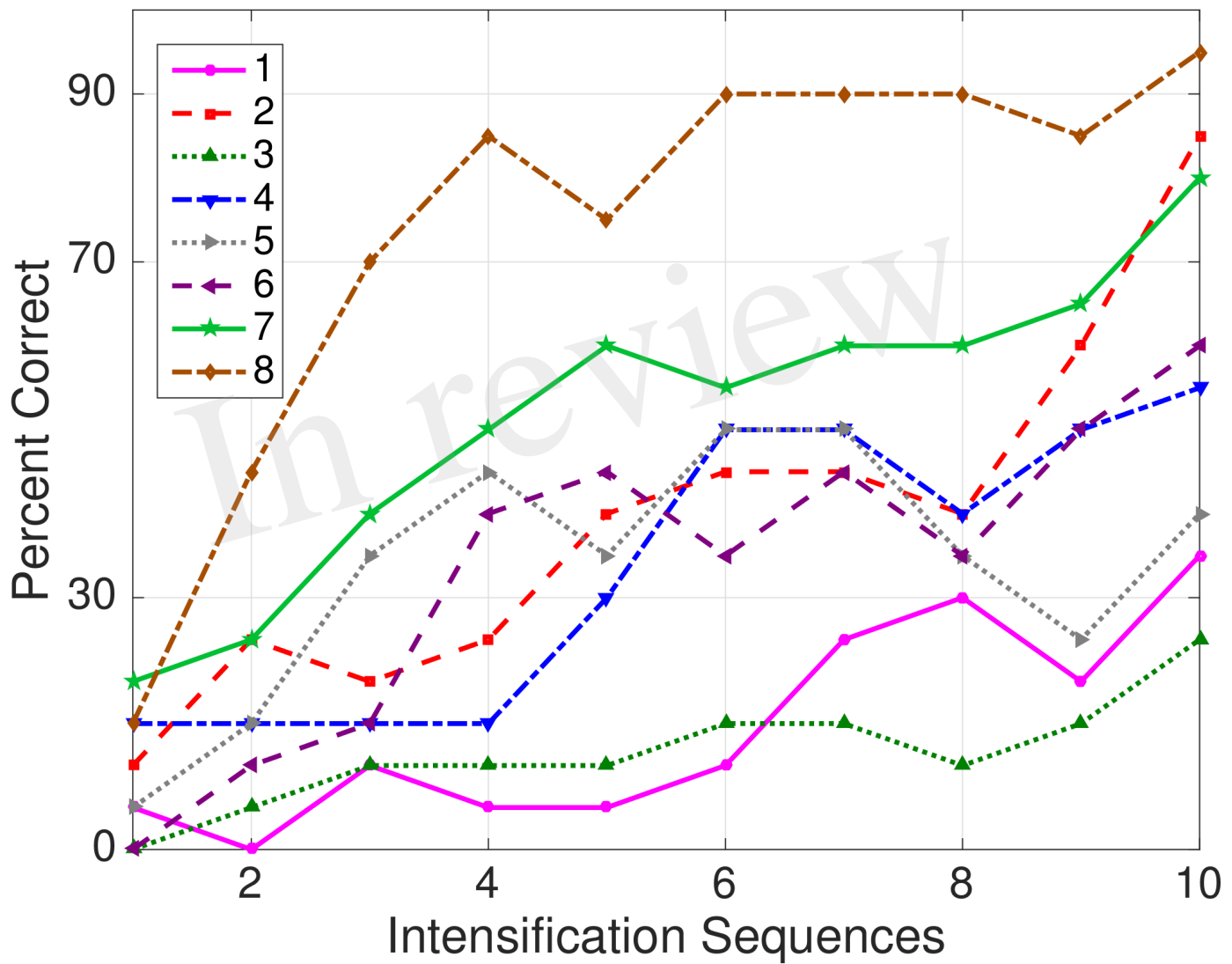


Figure 6.TIF

